Proton-proton bremsstrahlung at 200 MeV

J. G. Rogers, J. L. Beveridge, D. P. Gurd,* and H. W. Fearing
TRIUMF, Vancouver, B.C., Canada V6T 2A3

A. N. Anderson,† J. M. Cameron, and L. G. Greeniaus
University of Alberta, Edmonton, Alberta, Canada T6G 2N5

C. A. Goulding‡ and C. A. Smith
University of Manitoba, Winnipeg, Manitoba, Canada R3T 2N2

A. W. Stetz
Oregon State University, Corvallis, Oregon 97331

J. R. Richardson
University of California, Los Angeles, California 90024

R. Frascaria
Institut de Physique Nucléaire, 91406 Orsay, France
(Received 23 June 1980)

The coplanar symmetric proton-proton bremsstrahlung cross section at 16.4° and 200 MeV incident proton energy has been measured. The data are compared with four theoretical calculations, and sizable discrepancies are found. The data are in better agreement with a soft photon calculation than with predictions based on the Hamada-Johnston or the Reid soft-core potential models. The differences between the realistic potential model calculations and the data do not seem to be entirely explained by reasonable variations of the off-shell behavior of the model potentials.

[NUCLEAR REACTIONS $pp \rightarrow pp\gamma$ $\sigma(\theta_\gamma)$ measured; compared to several model calculations.]

I. INTRODUCTION

The interest in doing nucleon-nucleon (NN) bremsstrahlung experiments and calculations has usually been to investigate the off-shell behavior of the NN interaction. This off-shell behavior is important because descriptions of the NN interaction based on *elastic* scattering data do not determine the observables in more complicated nuclear systems, where one or both nucleons are not free. Among the measurable nonelastic observables, those for pp bremsstrahlung ($pp\gamma$) require the fewest approximations to calculate theoretically, and are therefore the most promising in which to study off-shell effects.

The standard procedure for extracting the off-shell information from $pp\gamma$ data is to calculate the expected $pp\gamma$ cross section using an NN model which describes adequately the elastic scattering data. If the predicted cross section does not fit the $pp\gamma$ data, then the model does not provide a realistic description of the NN interaction. In practice, it is not a simple matter to say that the failure of a model to fit $pp\gamma$ data is definitely due to off-shell effects. This is because different popular NN models do not give equally good fits to the elastic data and therefore do not have exactly the same on-shell behavior. A realistic model must fit the $pp\gamma$ data as well as the elastic data.

For this experiment the bombarding energy of 200 MeV was selected because it is high enough that the calculations show significant model sensitivity,[1] yet low enough so that relativistic effects can be approximately included as a correction in potential model calculations.[2-4] At a given bombarding energy, increasing off-shell effects at smaller proton scattering angles is a common qualitative feature of several $pp\gamma$ calculations. The calculations of Heller and Rich[5] showed that model off-shell effects increase dramatically as the angles get smaller. However, there are differences among the calculations regarding the details of how the sensitivity changes as a function of the proton emission angle. This is important for experimentalists because the choice of "best" angles involves a trade-off between greater model sensitivity at smaller angles versus a much easier experimental situation at larger angles.

The $pp\gamma$ cross section is very small compared with the pp elastic cross section. This results in a severe experimental background problem and

makes $pp\gamma$ cross section measurements difficult and expensive in terms of accelerator beam time. The symmetric proton angles chosen, $16.4° \pm 2.7°$, were the smallest values at which the experimental background situation was manageable.

The present article contains a description of the computer techniques used to analyze the data and a comparison of the resulting differential cross section with various theoretical calculations. The cross sections presented here supersede the preliminary results presented earlier[6] and analyzed in several theoretical papers.[7-10] These data differ somewhat from the earlier results due to improvements made in the data analysis. A brief description of the apparatus and experimental technique is contained in Ref. 6, and a complete description in Ref. 11.

II. DATA ANALYSIS

A. Processing the raw data tapes

Thirty raw data tapes were recorded by a Honeywell 316 data acquisition computer over a five-day period for subsequent analysis off-line. A simplified flow diagram of the off-line computer analysis procedure is shown in Fig. 1. The raw data tapes were read by the PPG program, which identified and treated events of two particular classes. All left-right coincidence events which had valid coordinates in all eight multiwire counter (MWC) planes were separated for subsequent analysis. Information on other events was summarized in the form of one- and two-dimensional histograms which were also saved for calibration purposes. These two classes of intermediate data produced by PPG were analyzed separately using the programs VERTEX and PPGNORM.

VERTEX was used to process the coincidence (i.e., $pp\gamma$ candidate) events into spectra of counts versus θ_γ (=the polar angle of the photon). Accidental and prompt background events were also separately processed in a similar manner to the $pp\gamma$ candidates. Processing included conversion of pulse heights[12] and times of flight into scattered energies, as well as computation of the trajectories of the protons from the MWC information. Consistency was required between the energy as measured by the pulse height and the energy as measured by time of flight for both of the two detected protons in each event. This eliminated events where one or both protons suffered a nuclear reaction in the counters and also prevented accidental coincidences of elastically scattered protons and background high-energy $(p, 2p)$ coincidences from being mistaken as $pp\gamma$ events. Such background elimination was the only use made of the time-of-flight information. In addition to the time-of-flight requirement described above, selection criteria used to identify $pp\gamma$ events also included the requirement that each proton trajectory originate in the gaseous target volume away from the walls and windows of the scattering chamber. The output of VERTEX consisted of several histograms of events which passed the selection criteria.

Figure 2(a) shows all the analyzed $pp\gamma$ candidates from VERTEX plotted as a function of their kinetic energies T_3 and T_4. In the absence of background, finite angular acceptance, and finite detector energy resolution, the events would be required by momentum conservation to be on a closed locus in the T_3, T_4 plane. Simulated $pp\gamma$ data generated

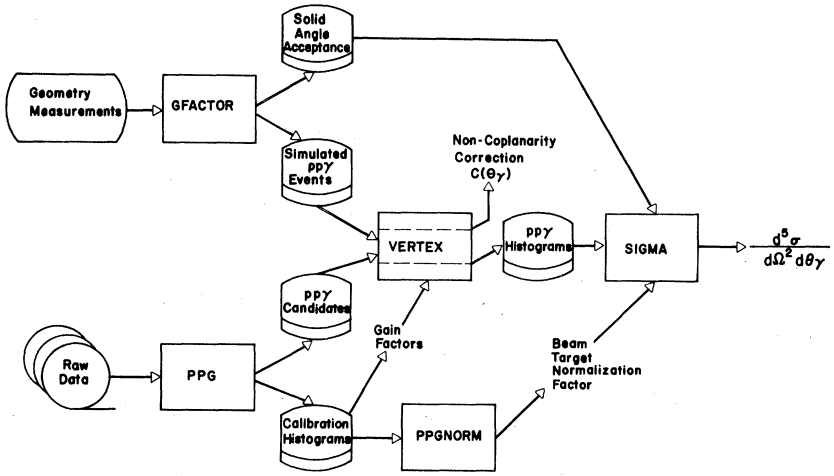

FIG. 1. A simplified flow chart of the computer processing used to analyze the data and determine the beam, target, and solid angle factors.

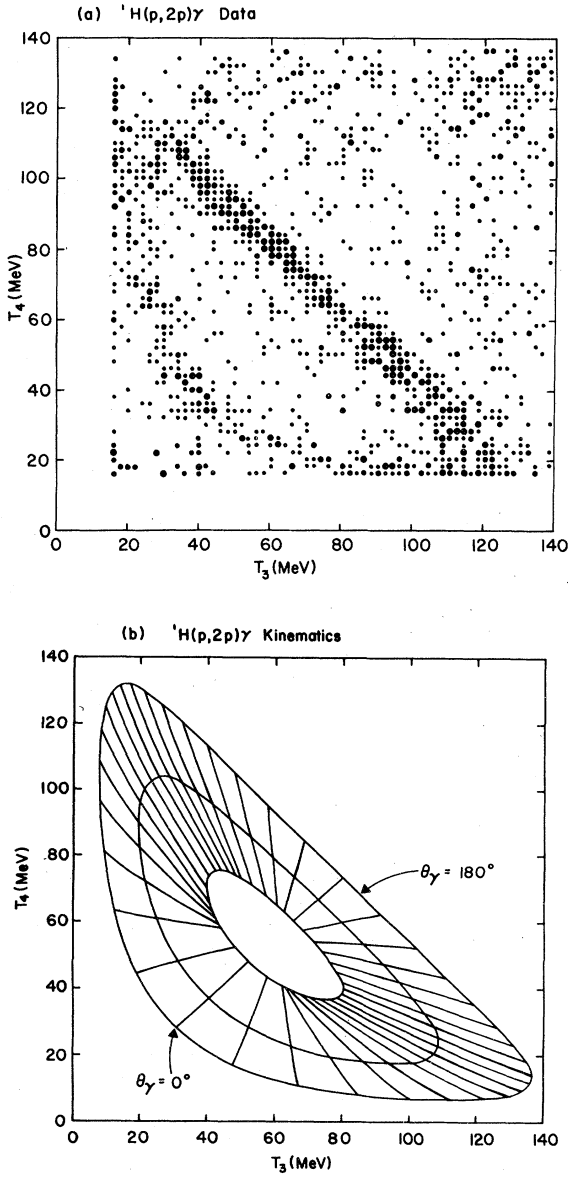

FIG. 2. (a) Prompt $pp\gamma$ data before background subtraction. (b) Contours of equal missing mass. Loci for missing mass = −50, 0, and 50 MeV are shown. Lines of constant θ_γ are shown at 10° intervals crossing the loci.

by a Monte Carlo program GFACTOR (see Fig. 1), which generated events randomly in the reaction volume viewed by the counter telescopes, show that the finite angular acceptance of the apparatus accounts for much of the observed broadening. These finite angular acceptance effects combine with an estimated ±5% energy resolution to smear the locus into a closed band. The events far from the expected $pp\gamma$ locus are background events. To separate events which satisfy the $pp\gamma$ kinematics from events which do not, a "missing mass" was computed for each of the $pp\gamma$ candidate events. For our purposes, missing mass was defined as

$$\text{missing mass} \equiv |\vec{p}_1 - \vec{p}_3 - \vec{p}_4|\, c - (T_1 - T_3 - T_4), \quad (1)$$

where $\vec{p}_1$, $\vec{p}_3$, and $\vec{p}_4$ are the measured 3-momenta of the incident and emerging protons and T_1, T_3, and T_4 are the corresponding measured kinetic energies. $\vec{p}_1$ is along the beam direction ($\theta_1 = 0°$). The directions of $\vec{p}_3$ and $\vec{p}_4$ were measured by the MWC detectors. Valid $pp\gamma$ events (i.e., events near the closed band) are characterized by missing mass near zero. Figure 2(b) shows kinematical contours of equal missing mass for the events which would be detected in the center of the detector system. Also shown in Fig. 2(b) are lines of constant θ_γ, which cross the contours like the spokes of a wheel.

Figure 3 shows three kinds of measured data plotted as a function of their computed missing mass. The solid line connects the data points for the prompt $pp\gamma$ candidates, including background events. The peak centered at zero missing mass contains the events which satisfy the $pp\gamma$ kinematics within the experimental resolution. Events with missing mass outside the limits −50 to 50 MeV were considered "background" events and rejected. Also shown are accidental coincidence events (dashed line) and prompt $(p, 2p)$ background plus accidental events (dotted line), which were analyzed in a similar manner to the real $pp\gamma$ data and eventually subtracted. The $(p, 2p)$ background data were acquired using an air target and normalized so that the combined backgrounds match the rejected $pp\gamma$ data (solid line) in the region between the vertical arrows in Fig. 3.

The finite angular acceptance does not contribute to uncertainty in the computation of θ_γ and missing mass for each event. This is because the

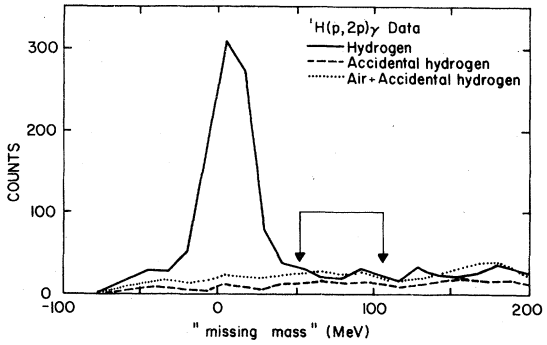

FIG. 3. A missing mass spectrum showing the prompt $pp\gamma$ data (solid line), accidental $pp\gamma$ data (dashed line), and normalized air + accidental $pp\gamma$ background data (dotted line). The air data were normalized over the region between the arrows.

precise trajectory of each event is measured by the MWC detectors. What contributes to the uncertainty in θ_γ and missing mass are the energy resolutions of the total energy detectors and multiple scattering. These resolution effects cause the distribution of events to have a finite width about the origin in the missing mass spectrum of Fig. 3. The θ_γ resolution turns out to be almost independent of θ_γ.

Figure 4 shows the spectrum of counts as a function of θ_γ for the events which satisfy a ±50 MeV missing mass criterion. The approximate left-right symmetry of the apparatus allows data from equal θ_γ bins to the left and right of the beam direction to be combined in the spectrum of Fig. 4 in order to improve statistics. This symmetry also implies reflection symmetry about the $T_3 = T_4$ line in Fig. 2. Also shown in Fig. 4 are the same two background spectra as in Fig. 3.

B. Determining the efficiency and normalization factors

To make comparison with theoretical calculations, the spectrum of counts versus θ_γ (Fig. 4) must be converted to a spectrum of cross section versus θ_γ. The cross section is related to the spectrum of counts by the formula

$$d^3\sigma/d\Omega^2 d\theta_\gamma = N(\theta_\gamma)/G(\theta_\gamma)\Delta\theta_\gamma \sum B_i \rho_i e_i , \qquad (2)$$

where $N(\theta_\gamma)$ is the spectrum of counts (see Fig. 4), $G(\theta_\gamma)$ is the solid angle factor, $\Delta\theta_\gamma$ is the bin size in the θ_γ spectrum (=15°), and B_i, ρ_i, and e_i are the integrated beam current, target density, and detection efficiency for the ith experimental run. The computation of the spectrum of counts, $N(\theta_\gamma)$, from the raw data was described in the last section.

The solid angle acceptance $G(\theta_\gamma)$ was computed from the measured counter sizes and positions using the program GFACTOR (see Fig. 1). This program performed a Monte Carlo integration of the geometrical acceptance by generating $pp\gamma$ events over the detector areas and along the line of intersection of the beam with the gas target. Multiple scattering and finite energy resolutions were neglected in computing the effective solid angle factor. The geometrical factor for a gas scattering coincidence experiment is conventionally[13] defined as

$$G = \int\int\int dz\, d\Omega_3 d\Omega_4 , \qquad (3)$$

where dz is an interval of target length along the line of intersection of the target and beam, and $d\Omega_3$ and $d\Omega_4$ are the solid angle elements accepted by the left and right detector systems. In our case the computation of the geometrical factor is complicated by the existence of the delta-ray suppression magnet between the target volume and the detectors and by the existence of a low energy cutoff in the detector telescopes. Instead of being the simple expression in Eq. (3), the range of integration used in computing G must be a function of the detected proton's energies as well as the usual geometrical counter sizes. For these reasons it was necessary to compute a differential $G(\theta_\gamma)$ as a function of θ_γ. It was convenient to include in $G(\theta_\gamma)$ all parts of the efficiency which depended on the proton energies (T_3 and T_4). Thus $G(\theta_\gamma)$ includes the inefficiency due to nuclear reactions in the detectors[14] as well as that due to the low energy threshold of the counters (15 MeV). The geometrical factor was computed separately for θ_γ to the left (0–180°) and right (180–360°) of the beam direction. The delta-ray suppression magnet and cyclotron fringe field combined to bend the low energy protons causing a slight left-right asymmetry in the geometrical acceptance factor $G(\theta_\gamma)$.[15] To calculate $G(\theta_\gamma)$ over the range 0–180° for Eq. (2), the geometrical factors were treated in the same way as the data, namely acceptances were added for equal values of θ_γ to the left and right of the beam. The resulting $G(\theta_\gamma)$ has an uncertainty of ±10% except in the region affected by the energy thresholds ($30 \lesssim \theta_\gamma \lesssim 70°$), where the uncertainty might be as high as ±20%. These are the major systematic uncertainties in the final experimental cross sections as computed from Eq. (2).

The normalization factor $\sum_i B_i \rho_i e_i$ in Eq. (2) was computed by using the program PPGNORM (see Fig. 1). The integrated beam current for each run, B_i in Eq. (3), was determined from a scattering monitor upstream of the target chamber.[6,11] This monitor has been calibrated against a Faraday cup to an absolute accuracy of better than ±2%. The hydrogen or air target density ρ_i was

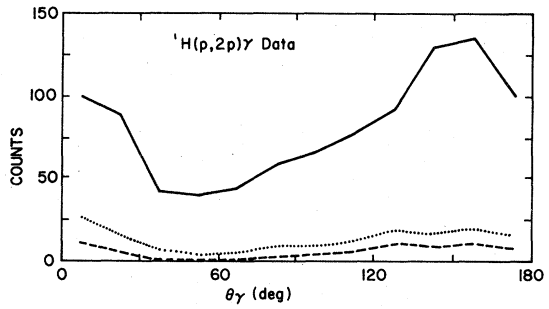

FIG. 4. Measured θ_γ spectrum of counts. Straight line segments join the data points which are binned (integrated) in 15° bins in θ_γ. The three data types are the same as in Fig. 3.

determined using the temperature and pressure from solid state transducers, which were automatically recorded by the acquisition computer at the end of each run. The portion of the efficiency which was independent of θ_γ, e_i in Eq. (2), was determined for each run utilizing the simultaneously measured elastic events. These events, which have known signatures in energy and time of flight, were analyzed to produce the efficiency of one telescope, excluding computer dead time. The coincidence counter efficiency was then assumed to be the square of the single arm efficiency.[16] The computer dead time was separately determined from scalar ratios. The combination of these effects for the thirty experimental runs yielded values of e_i ranging from 0.48 to 0.71.[17]

As a check on the computation of the efficiency, e_i was independently computed by another method. Simultaneously acquired pulser events, which simulate the $pp\gamma$ coincidence events in time structure, were analyzed identically to the real $pp\gamma$ events. The detection efficiency was then computed as the fraction which survive the entire analysis. This efficiency accounts for counter and computer dead time and pileup losses. The two methods of computing the efficiency were in good agreement for most of the thirty runs.

As an additional check on the overall data normalization, we computed the elastic hydrogen differential cross section from the elastic data recorded with each run. This provided a check that no important factors affecting the normalization were overlooked. The thirty experimental runs yielded elastic cross section measurements with a total spread of ±2%, with an average value which agrees with the known[18] differential cross section within 0.5%. The combined uncertainty in efficiencies and beam-target normalization is estimated to be ±2%, which is negligible compared to errors in $G(\theta_\gamma)$.

The final step in the analysis procedure, as indicated in Fig. 1, was performed using the program SIGMA. The final step involved combining the $pp\gamma$ and background histograms produced by VERTEX with proper normalizations from PPGNORM and GFACTOR to produce the spectrum of cross section versus θ_γ. This cross section is tabulated in Table I. The tabulated uncertainties include all the known sources of possible error, both systematic and statistical, added in quadrature. The major source of systematic error is the uncertainty in the Monte Carlo calculation of the geometrical factor (described above). Statistical errors are typically 10–15% of the measured cross section (see Fig. 4).

III. COMPARISON WITH THEORY

A. Distortion due to experimental acceptances

The experimental data were compared with several theoretical calculations. These calculations all make predictions of the cross section $(d^3\sigma/d\Omega^2 d\theta_\gamma)$ as a function of the laboratory polar angle of the photon (θ_γ) for fixed proton angles. The experimental apparatus, however, measures the cross section *averaged* over a range of proton and

TABLE I. Experimental cross section and computed cross sections as a function of θ_γ.

θ_γ (deg)	Experiment (μb/sr$^2\gamma$)	Correction [a] σ_{ave}/σ_c	Soft photon [c] (μb/sr$^2\gamma$)	Reid [d] (μb/sr$^2\gamma$)	Hamada-Johnston [d] (μb/sr$^2\gamma$)	BA-OBE [e] (μb/sr$^2\gamma$)
0.0			0.454	0.84	0.73	0.73
7.5	0.65±0.11	1.05 [b]	0.468	0.87	0.76	0.73
22.5	0.60±0.10	1.06	0.522	0.93	0.85	0.68
37.5	0.32±0.08	1.06	0.499	0.74	0.71	0.56
52.5	0.36±0.10	1.06	0.411	0.52	0.52	0.44
67.5	0.34±0.08	1.07	0.329	0.37	0.37	0.36
82.5	0.34±0.07	1.08	0.323	0.34	0.33	0.35
97.5	0.45±0.08	1.10	0.430	0.50	0.45	0.42
112.5	0.78±0.12	1.09	0.635	0.79	0.69	0.58
127.5	0.79±0.13	1.07	0.865	1.10	0.97	0.84
142.5	0.96±0.15	1.06	1.038	1.38	1.22	1.17
157.5	1.06±0.15	1.07	1.111	1.57	1.37	1.48
172.5	0.81±0.13	0.99 [b]	1.145	1.58	1.38	1.68
180.0			1.152	1.55	1.36	1.72

[a] Computed from SPA as explained in the text.
[b] Includes additional corrections from Monte Carlo Calculation. See Appendix for details.
[c] H. W. Fearing, Ref. 7.
[d] G. E. Bohannon, Refs. 20 and 21.
[e] Adam Szyjewicz and A. N. Kamal, Ref. 22.

photon angles, namely the range of proton angles accepted by the counter system and the bin size selected for the θ_γ spectrum (=15°). To make a comparison, the theoretical calculations must also be averaged to take account of these finite acceptances. To investigate the importance of these averaging effects we performed a numerical integration of the soft photon approximation (SPA) (Ref. 19) cross section using a 12-point integration mesh over the acceptance of the counter system. Figure 5 shows the SPA prediction averaged over the experimental solid angle acceptance, as well as the SPA calculated for point geometry at the central angles of the detector system. The figure shows that averaging over the acceptance changes the cross section very little except near $\theta_\gamma = 0°$ and 180°.

To provide theorists with a convenient means of accounting for these finite acceptance effects, we computed a correction factor which can be applied to calculations done for point geometry. This correction factor was taken to be the ratio of the averaged SPA cross section to the SPA cross section computed at the center of the acceptance. This factor is tabulated as the third column in Table I. The coarse-step integration procedure described above was found to be inaccurate near the ends of the θ_γ spectrum ($\theta_\gamma = 0°$ and 180°), so that a more elaborate Monte Carlo integration procedure was employed to calculate the first and last entries in the column of correction factors. See the Appendix for the details of this calculation.

Also shown in Table I are the theoretical cross sections from four different calculations, namely the SPA,[19] Reid soft core potential model (R),[20] Hamada-Johnston potential model (HJ),[21] and a Born approximation to a one-boson-exchange model (BA-OBE) (Ref. 22) calculation. The four tabulated (i.e., not averaged) theoretical cross sections were computed for point geometry at $\theta_3 = \theta_4 = 16.4°$ and $\phi_3 - \phi_4 = 180°$. The finite acceptance effects may be accounted for by multiplying the tabulated theoretical cross sections by the correction factor, as discussed above. Figure 6 shows the measured cross section as points with error bars, along with the four corrected calculations. The calculations are discussed in detail below.

There are significant differences between the final data spectrum presented in Table I and Fig. 6 and the "preliminary data" spectrum presented earlier in Ref. 6. These differences, which occur mainly in the region $\theta_\gamma = 135°-180°$, are believed due to an erroneously small normalization for the air background which was subtracted in the preliminary analysis. The error in the background subtraction combined with a greater uncertainty in the energy calibration in the preliminary analysis to cause the preliminary data spectrum in Ref. 6 to be contaminated in the region $\theta_\gamma = 135°-180°$.

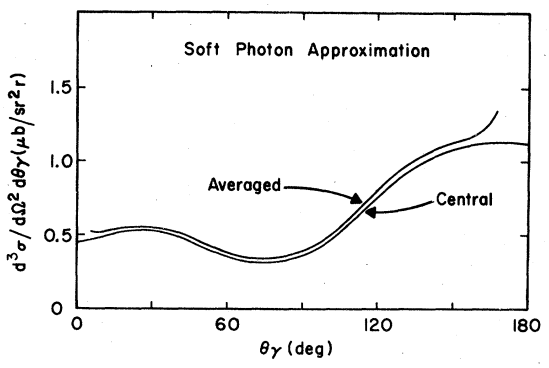

FIG. 5. The effect of the finite geometrical acceptance of the counters. The upper curve is the SPA averaged over the actual finite acceptances and the lower curve is the same calculation without averaging.

B. Soft photon approximation

The cross section for the $pp\gamma$ process may, in general, be written as[23]

$$d^3\sigma/d\Omega^2 d\theta_\gamma = A^2/k + 2\,\mathrm{Re}AB^* + (B^2 + 2\,\mathrm{Re}AC^*)k + O(k^2), \quad (4)$$

where k is the photon momentum and A, B, and C are coefficients arising from expansion of the $pp\gamma$ amplitude about the on-shell ($k=0$) point. The A and B coefficients contain kinematic factors and purely on-shell (elastic) information, while C and the higher-order coefficients contain

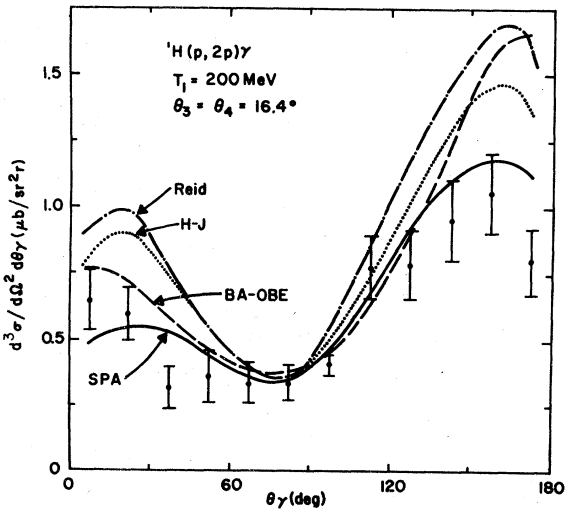

FIG. 6. The measured $pp\gamma$ cross sections (with error bars) and calculated theoretical cross sections. The calculations are discussed in the text.

off-shell information, as well as on-shell contributions. The approximation involved in the SPA approach is to compute the cross section assuming that C and all $O(k^2)$ terms are negligible. Comparison of the SPA cross section with data therefore tests this assumption.

As pointed out by Fearing earlier,[7] since the A and B coefficients contain only on-shell information, sensitivity to off-shell effects requires at least that the cross section in Eq. (4) have significant contributions from the terms of $O(k)$ and higher. For our geometry the SPA cross section is dominated by the B^2k term, in contrast to the situation in experiments at lower energies.[7]

The SPA, of all the four calculations, agrees best with our data, as seen in Fig. 6. Analyses of other experiments in this energy range, namely those at 158 and 204 MeV (Ref. 24) and at 156 MeV (Ref. 25), are also consistent with this qualitative agreement with SPA. However, it should be noted that these other experiments were performed at different angles and are generally subject to larger experimental uncertainties than the present work. At much lower energy (42 MeV) (Refs. 26 and 25) the coplanar data tend to fall above SPA but below potential model calculations, and thus fit the two equally well. At higher energy (730 MeV),[27] the data tend to fall increasingly *above* SPA, as k increases in contrast to the situation here at 200 MeV.

An essential test which has not yet been done is to investigate the "prescription dependence" of the SPA calculation, i.e., the change in the cross section which would result if the *NN* elastic amplitudes in the SPA were evaluated at a different energy and momentum transfer. The B^2 term in Eq. (4), which dominates the cross section, is the same order in k as the AC term, the lowest order term containing prescription dependence. [Note, however, that because of our symmetrical geometry, $A \equiv 0$ at $\theta_\gamma = 0$ and 180°,[7] so the effects of prescription dependence at the end points of the θ_γ spectrum would first appear in terms of $O(k^2)$ rather than $O(k)$.] The prescription used in the SPA results presented in this paper is the "average energy" prescription of Nyman.[24] Other prescriptions have been suggested by Feshbach and Yennie[28] and recently by Heller.[10] The prescription dependence of the SPA calculation is being investigated by one of us (H. W. F.).

C. Potential model calculations

The potential model calculations were performed by Bohannon[20,21] using the Reid soft core and Hamada-Johnston *NN* potentials. These calculations are of the type developed extensively for comparison with data in the low-energy domain,[29] and have been extended to intermediate energies using the relativistic spin correction developed by Liou and Sobel.[2,30] Figure 7 shows the magnitude of these relativistic correction factors for our kinematic situation. It is somewhat worrisome that the relativistic corrections are so large (30% for backward-going photons), as the correction cannot be made in an entirely consistent way.

In these potential model calculations the *NN* amplitudes are obtained from potentials via the Schrödinger equation, which is inherently nonrelativistic. However, since the potentials are obtained by a phenomenological fit to elastic data, they mock up some of the relativistic effects in the *NN* scattering, but in a not very well defined way. These and other complications involved with relativistic corrections are discussed in the paper of Liou and Sobel.[2] Although it is difficult to assign a precise uncertainty due to relativistic effects, it seems very unlikely that it could be large enough to account for the observed discrepancy between the potential model calculations and the data.

Thus we conclude that *neither the Reid nor the Hamada-Johnston NN potentials used in the best currently available ppy calculations give an adequate description of the ppγ cross section* for our kinematical situation.

The first question we should ask at this point is whether or not the discrepancy between the potential model calculation and the data can be accounted for by reasonable off-shell effects. The question of the sensitivity of the calculated cross section to the *NN* potential has been studied by Heller and Rich[5] and separately by Bohannon[31] using phase-equivalent transformations of the Hamada-Johnston and Reid potentials.

The difference between the Hamada-Johnston calculation and the data is about 25% in the inte-

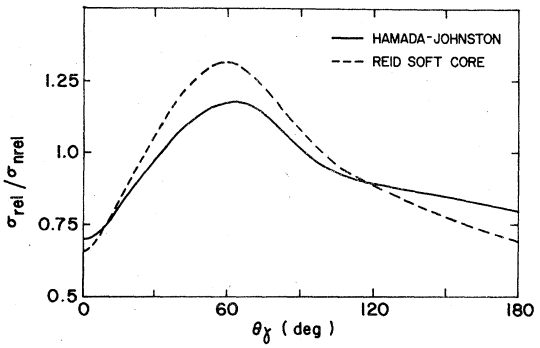

FIG. 7. Relativistic corrections computed by Bohannon (Ref. 20) for the Reid (R) and Hamada-Johnston (HJ) potential models. The ordinate scale is the ratio of the corrected to uncorrected differential cross section. σ_{rel} is tabulated in Table I for the two models.

grated ($d^2\sigma/d\Omega^2$) cross section (2.5 and 1.9 μb/sr^2, respectively). From the work of Heller and Rich[5] using phase-equivalent transformations of the Hamada-Johnston potential, it appears at first glance that an off-shell variation of this size would be obtainable with the maximum allowable phase-equivalent distortion of the Hamada-Johnston potential. (The transformation is characterized by $S=7.0$ in the notation of Heller and Rich.) This is necessarily a tentative conclusion, as it requires an extrapolation from their published 158 MeV result to our 200 MeV kinematical situation.

For the Reid soft core potential the calculated cross section ($d^2\sigma/d\Omega^2=3.0$ μb/sr^2) is about 60% larger than the measured cross section. Phase-equivalent transformations of the Reid potential have been studied by Bohannon[30] using a separable form. The maximum variation of the cross section obtained (with Bohannon's parameter $\alpha=8$) at 200 MeV was too small to account for the observed 60% discrepancy. The transformations studied by Bohannon have a different functional form from those of Heller and Rich, but it seems doubtful that much larger variations are possible with any form involving only one adjustable parameter.

Sauer[32] has criticized the phase-equivalent transformations of the type used by Bohannon because no effort was made to preserve the *NN* scattering lengths and because the nonlocalities introduced by the transformation make the effective velocities not small compared to c, which means that relativistic corrections would be large if they were included. It is not known whether such criticisms apply to the Baker transformation[33] used by Heller and Rich, although it seems at least probable that the scattering lengths are not preserved by their transformation either.

We can also ask a qualitative question which is roughly equivalent to the quantitative questions raised by Sauer, a question that can be answered by examining the transformed wave functions. The question is: "Do the transformations produce a 'reasonable' transformed wave function?" The main criterion for a reasonable wave function is that it should agree with the untransformed wave function at large and intermediate distances, where the wave function itself is believed to have a particular form because the interaction is due to one- and two-pion exchanges. From the work of Vinh Mau[34] we know that one- and two-pion exchange contributions fix the wave function at internucleon distances larger than 0.8 fm.

Heller has shown[35] that the required Baker transformation[5] of the Hamada-Johnston potential does *not* produce a reasonable wave function in the $^1S_0$ state. The transformed wave functions do have substantial variations outside of 0.8 fm and therefore must be rejected. Thus it appears that the differences between the data and the potential model calculations are too large to be accounted for by reasonable phase-equivalent transformations of the potentials, at least not the type of transformations studied so far.

Thus we are left with the situation that the discrepancies between potential model calculations and data appear to be *too large* to be due to purely off-shell effects. However, we must recognize that the potential model description of the interaction is incomplete, as it does not include radiation from the exchanged bosons which are believed to be responsible for the interaction. In particular, we know that the computed cross section at this energy depends sensitively on the wave function inside of 0.8 fm,[36] where the interaction is dominated by two- and three-pion exchanges. These exchanges involve charged pions which may themselves radiate, as well as radiation from nucleon isobars. Whether this type of radiation or some other effect is causing the large discrepancy between data and potential model calculations cannot be determined without additional calculations.

D. One-boson-exchange (OBE) model

The basic concept behind the OBE model is esthetically more pleasing than the potential models. The *NN* force, on and off the energy shell, is believed to be related to the exchange of more fundamental particles between the nucleons. The phenomenological potential models discussed in the previous section do not incorporate these features, except for the one-pion exchange which governs only the very longest range part of the interaction. The formulation of the OBE model for $pp\gamma$ calculations has received much less attention than the potential model calculations described above. Until quite recently there was only a single publication in the literature, namely the pioneering work of Baier, Kuhnelt, and Urban.[37] This type of calculation has several advantages over potential model calculations in our intermediate-energy domain: (1) The model is covariant and gauge invariant; (2) meson exchange current contributions can be partially included; (3) two-step processes, such as $pp \to p\Delta \to pp\gamma$, can be included.

The major disadvantage is that the model has only been applied so far in Born approximation. The calculation does not include the iteration of the interaction that is performed in the potential model approach to $pp\gamma$ by solving the Schrödinger equation. Unlike the OBE model analysis of elastic scattering,[38] which uses the Lippmann-Schwinger equation to provide unitarity, this Born ap-

proximation (BA-OBE) is not unitary and is therefore not a good description of the on-shell (elastic) scattering. Within the framework of the Born approximation there is no satisfactory way of repairing this error due to nonunitarity. Such a repair was attempted by Szyjewicz[39] in adjusting the model form factors and cross section normalization to fit the elastic differential cross section, but this technique is unsatisfactory, as the resulting *NN* model is not related to known meson exchanges.

Nevertheless the BA-OBE model results contain valuable qualitative information. The internal radiation represented by the ω-production diagram in Fig. 8(a) contributes about ±10% to the model $pp\gamma$ cross section for our kinematics. On the other hand, intermediate Δ production [diagram 8(b)] is estimated to be negligible at this energy compared to the normal external emission diagrams [Fig. 8(c)], which make the major contribution to the cross section. Neither of the effects represented by the diagrams 8(a) and 8(b) is included in the potential model calculations discussed earlier. These results of the BA-OBE model calculations[39,40] imply that including meson exchange currents contributions would be required in any potential model calculation purporting to give results believable at the ±10% level.

IV. SUMMARY AND CONCLUSIONS

We have performed a measurement of proton-proton bremsstrahlung ($pp\gamma$) at 200 MeV and symmetric angles. Potential model calculations for our geometry show much larger differences from model to model than has been observed in kinematic regions where other experiments have been done. However, none of the three models we tested (Reid, Hamada-Johnston, BA-OBE) agreed with the measured cross section. Rather the cross section is in fair agreement with an SPA, which is quite surprising in view of the high degree of inelasticity of this experiment.

The lack of agreement between the potential models (Reid and Hamada-Johnston) and the data does not seem to be a purely off-shell effect. Rather (we infer) calculations with potentials phase equivalent to the Reid and Hamada-Johnston potentials would still disagree with the data. More theoretical calculations employing phase-equivalent transformations and more realistic potentials (like the Paris potential[34]) are definitely called for.

In addition it seems very important to examine the potential models carefully as they apply to our rather extreme kinematic conditions. Are there approximations made, such as ignoring Coulomb effects, rescattering, and higher partial waves, which are inaccurate for these conditions? Are there real processes omitted from the potential models, e.g., internal radiation from exchanged pions, which would be required to describe the reaction accurately? These are questions we must leave to the theorists to consider.

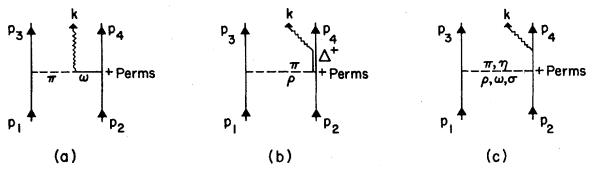

FIG. 8. Diagrams which have been included in the BA-OBE model calculation. (a) Internal radiation from ω decay. (b) Radiation from intermediate Δ production. (c) Normal (dominant) external radiation from the four nucleon lines.

ACKNOWLEDGMENTS

We thank J. V. Jovanovich for essential assistance in acquiring the data analyzed in this paper. For invaluable discussions we thank Leon Heller, B. F. Gibson, G. E. Bohannon, Adam Szyjewicz, A. N. Kamal, and M. K. Liou. We thank Dr. Bohannon, Dr. Heller, Dr. Szyjewicz, and Dr. Kamal for providing us with valuable results of unpublished or to-be-published calculations. This work was supported in part by the National Research Council of Canada through the office of Grants and Scholarships.

APPENDIX: MONTE CARLO ACCEPTANCE AVERAGING

For noncoplanar portions of the acceptance ($\phi_3 - \phi_4 \neq 180°$), the calculated differential cross section ($d^3\sigma/d\Omega^2 d\theta_\gamma$) has singularities at the smallest and largest kinematically allowed values of θ_γ. For small departures from coplanarity, such as that accepted by our apparatus, the singularities occur close to $\theta_\gamma = 0°$ and $\theta_\gamma = 180°$, so effects on the average cross section are confined to the extreme 25° at the ends of the θ_γ spectrum. The sudden rise of the average cross section seen in Fig 5 is due to a breakdown of the coarse-mesh averaging procedure (described in Sec. III A) in the vicinity of the singularities near $\theta_\gamma = 180°$. The effects of the finite acceptance at the ends of the θ_γ spectrum were determined using a Monte Carlo technique as described below.

To avoid the expense of calculating the SPA cross section at a large number of mesh points, the simplest functional form (e.g., a constant) was used for the cross section in averaging over the acceptance. Monte Carlo events were generated

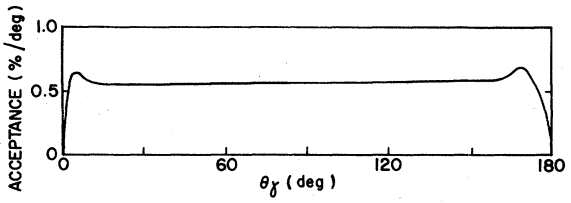

FIG. 9. Acceptance function calculated by Monte Carlo techniques (described in the text). The rise and fall of the acceptance near the end points are due to phase-space singularities and smaller solid angles for nearly coplanar events.

uniformly in θ_3, θ_4, ϕ_3, ϕ_4, and the projected photon angle $[=\tan^{-1}(\tan\theta_\gamma \cos\phi_\gamma)]$ using the program GFACTOR (see Fig. 1). These events were formed into a spectrum as a function of θ_γ using the program VERTEX. The resulting distribution is shown in Fig. 9. For coplanar geometry the projected photon angle is equal to θ_γ, so the constant cross section has the convenient feature that the point geometry cross section is a constant in θ_γ. The spectrum shown in Fig. 9 was integrated in 15° bins to determine the correction factor for the end bins in the θ_γ spectrum relative to the central bins. To include the effects of cross section variations, the central bin averages were determined from the more rigorous SPA averaging (described in Sec. III A) and multiplied by the relative correction factor (from Fig. 9) to determine the overall corrections for the end bins. The overall correction factor is shown in Table I. The Monte Carlo technique described in this appendix was used to compute the first and last entries in the "correction" column of Table I.

---

*University of Alberta.
†Permanent address: EGG Idaho Inc., Idaho Falls, Idaho 83401.
‡Present address: LAMPF, Los Alamos, New Mexico 87545.

[1]V. R. Brown, Phys. Rev. 177, 1498 (1969).
[2]M. K. Liou and M. I. Sobel, Ann. Phys. (N.Y.) 72, 323 (1972).
[3]L. S. Celenza, M. K. Liou, M. I. Sobel, and B. F. Gibson, Phys. Rev. C 8, 838 (1973).
[4]B. F. Gibson, private communication.
[5]L. Heller and M. Rich (unpublished); L. Heller, in *Few Body Problems in Nuclear and Particle Physics*, edited by R. J. Slobodrian, B. Cujec, and C. Ramavataram (Les Presses de l'Université Laval, Québec, 1975), p. 206; W. T. H. Van Oers, *ibid.*, p. 307.
[6]J. L. Beveridge, D. P. Gurd, J. G. Rogers, H. W. Fearing, A. N. Anderson, J. M. Cameron, L. G. Greeniaus, C. A. Goulding, J. V. Jovanovich, C. A. Smith, A. W. Stetz, J. R. Richardson, and R. Frascaria, *Nucleon-Nucleon Interactions—1977 Vancouver*, Proceedings of the Second International Conference on Nucleon-Nucleon Interaction, edited by D. F. Measday, H. W. Fearing, and A. Strathdee (AIP, New York, 1978), p. 446.
[7]H. W. Fearing, Ref. 6, p. 506.
[8]G. E. Bohannon, Bull. Am. Phys. Soc. 23, 552 (1978).
[9]A. Szyjewicz and A. N. Kamal, in *Few Body Systems and Nuclear Forces—I*, proceedings of the VIII International Conference on Few Body Systems and Nuclear Forces, Graz, 1978, edited by H. Zingl, M. Haftel, and H. Zankel (Springer, Berlin, 1978), p. 88.
[10]Leon Heller, in *Few Body Systems and Nuclear Forces—II*, proceedings of the VIII International Conference on Few Body Systems and Nuclear Forces, Graz, 1978, edited by H. Zingl, M. Haftel, and H. Zankel (Springer, Berlin, 1978), p. 68.
[11]J. V. Jovanovich, C. A. Goulding, C. A. Smith, J. G. Rogers, J. L. Beveridge, D. P. Gurd, H. W. Fearing, A. N. Anderson, J. M. Cameron, L. G. Greeniaus, A. W. Stetz, J. R. Richardson, and R. Frascaria (unpublished).
[12]The conversion of pulse height to scattered energy was complicated by the inherent nonlinearity of the plastic scintillator material and by the light collection efficiency of the detectors, which varied as a function of position across the face. The light collection efficiency as a function of position was measured in a separate experiment. The scintillator response function at low energies was taken from the literature: T. J. Gooding and H. G. Pugh, Nucl. Instrum. Methods 7, 189 (1960); R. L. Craun and D. L. Smith, *ibid.* 80, 239 (1970).
[13]J. G. Rogers, Ph.D. thesis, UCLA, 1969 (unpublished); E. Bar-Avraham and L. C. Lee, Nucl. Instrum. Methods 64, 141 (1968).
[14]D. F. Measday and C. Richard-Serre, CERN Report No. 69-17, 1969.
[15]Owing to the asymmetry in $G(\theta_\gamma)$, our measurement is not precisely a symmetric $pp\gamma$ experiment. However, the departure from symmetry is so small that negligible error was introduced by averaging the left and right data. Without averaging the proton scattering angles would have been $\theta_{\text{left}} = 16.1 \pm 2.6°$ and $\theta_{\text{right}} = 16.8 \pm 2.7°$.
[16]Due to an equipment malfunction, useful elastic events were acquired in only one of the two telescopes. The efficiencies of the two telescopes were later measured to be equal over a wide range of conditions, as expected.
[17]The inefficiency is almost entirely due to unresolved multiple tracks in the eight MWC detectors due to the high rate of elastically scattered protons.
[18]The laboratory pp elastic cross section was computed by C. A. Miller of the University of Alberta using the phase shifts of R. A. Arndt, R. H. Hackman, and L. D. Roper, Phys. Rev. C 9, 555 (1974).
[19]The SPA calculations were performed by one of us (H.W.F.) as described in Ref. 7.
[20]G. E. Bohannon, private communication and Ref. 8.
[21]Hamada-Johnston potential model calculations were performed both by Bohannon (Ref. 20) and by M. K. Liou and B. F. Gibson (Refs. 3 and 4). The calculation

of Bohannon is 0–9% larger than that of Liou and Gibson. Table I contains the Hamada-Johnston calculation of Bohannon.

[22]The BA-OBE model was calculated by Adam Szyjewicz and A. N. Kamal, see Ref. 6, p. 502, and Ref. 9.

[23]F. E. Low, Phys. Rev. 110, 974 (1958).

[24]E. M. Nyman, Phys. Rev. 170, 1628 (1968), and references to experiments therein.

[25]H. W. Fearing, Phys. Rev. C 22, 1388 (1980) and Ref. 7.

[26]C. A. Smith, J. V. Jovanovich, and L. G. Greeniaus, Phys. Rev. C (to be published).

[27]B. M. K. Nefkens, O. R. Sander, and D. I. Sober, Phys. Rev. Lett. 38, 876 (1977); B. M. K. Nefkens, O. R. Sander, D. I. Sober, and H. W. Fearing, Phys. Rev. C 19, 877 (1979).

[28]H. Feshbach and D. R. Yennie, Nucl. Phys. 37, 150 (1962).

[29]M. L. Halbert, in *The Two Body Force in Nuclei*, edited by S. M. Austin and G. M. Crawley (Plenum, New York, 1972), p. 53.

[30]The relativistic corrections included by Bohannon are actually more extensive than those used in Ref. 3. See Ref. 20.

[31]G. E. Bohannon, Ref. 6, p. 482 and Ref. 10.

[32]P. U. Sauer, Ref. 6, p. 195; Phys. Rev. C 11, 1786 (1975).

[33]G. A. Baker, Phys. Rev. 128, 1485 (1962).

[34]R. Vinh Mau, Ref. 6, p. 140; M. Lacombe, B. Loiseau, J. M. Richard, R. Vinh Mau, J. Côté, P. Pirès, and R. de Tourreil, Phys. Rev. C 21, 861 (1980).

[35]Leon Heller, private communication and Ref. 10.

[36]G. E. Bohannon, Ref. 6, p. 494.

[37]R. Baier, H. Kuhnelt, and P. Urban, Nucl. Phys. B11, 675 (1969).

[38]K. Erkelenz, K. Holinde, and R. Machleidt, Phys. Lett. 49B, 209 (1974).

[39]Adam Szyjewicz, private communication and Ph. D. thesis, University of Alberta, 1979.

[40]The contribution from ω decay is reported in A. Szyjewicz and A. N. Kamal, Nucl. Phys. A285, 397 (1977). See also Refs. 22 and 39.